

Speed of sound and polytropic index in QCD matter

He Liu,^{1,2,*} Chi Yuan,³ Yong-Hang Yang,^{1,2} Min Ju,^{4,†} Xu-Hao Wu,^{5,‡} and Peng-Cheng Chu^{1,2,§}

¹*Science School, Qingdao University of Technology, Qingdao 266520, China*

²*The Research Center of Theoretical Physics, Qingdao University of Technology, Qingdao 266033, China*

³*School of Mechanical and Automotive Engineering,*

Qingdao University of Technology, Qingdao 266520, China

⁴*School of Science, China University of Petroleum (East China), Qingdao 266580, China*

⁵*School of Science, Yanshan University, Qinhuangdao 066004, China*

(Dated: November 17, 2023)

We investigate the speed of sound and polytropic index of quantum chromodynamics (QCD) matter in the full phase diagram based on a 3-flavor Polyakov-looped Nambu–Jona-Lasinio (pNJL) model. The speed of sound and polytropic index in isothermal and adiabatic cases all have a dip structure at the low chemical potential side of the chiral phase transition boundary, and these quantities reach their global minimum values at the critical endpoint (CEP) but are not completely zero, where the values in adiabatic are lightly greater than those in isothermal. Different from the speed of sound, the polytropic index also exists a peak around the chiral phase transition boundary. Along the hypothetical chemical freeze-out lines, the speed of sound rapidly decreases near the CEP, followed by a small spinodal behavior, while the polytropic index, especially in isothermal, exhibits a more pronounced and nearly closed to zero dip structure as it approaches the CEP.

PACS numbers: 21.65.-f, 21.30.Fe, 51.20.+d

Exploring the phase structure of quantum chromodynamics (QCD) matter and searching for the signals of the phase transition are significant goals in both theoretical research and heavy-ion collision experiments. Lattice QCD (LQCD) simulations indicate the transition between the quark-gluon plasma (QGP) and the hadronic matter is a smooth crossover at nearly zero baryon chemical potential (μ_B) [1–3]. A first-order phase transition, with a critical endpoint (CEP) connecting with the crossover transformation, is predicted at large baryon chemical potential by the various effective quark models, e.g., Nambu–Jona-Lasinio (NJL) model, quark-meson (QM) model, Dyson-Schwinger equation (DSE) and functional renormalization group (FRG) approaches [4–13]. In order to find the signal of the QCD CEP at finite μ_B , the Beam Energy Scan (BES) program is currently ongoing at the Relativistic Heavy-Ion Collider (RHIC) [14, 15]. In the BES program, the STAR experiment has measured the energy dependence of observables that are sensitive to the CEP and/or first-order phase transition, including net-proton fluctuations [16, 17], pion HBT radii [18, 19], baryon directed flow [20, 21], intermittency of charged hadrons [22], and light nuclei yield ratio ($N_t \times N_p / N_d^2$) [23–26]. Nonmonotonic energy dependencies were observed in all of these observables, and the energy ranges where peak or dip structures appear are around $\sqrt{sNN} \approx 7.7 - 39$ GeV. Those provoking observations are of great interest, and more accurate measurement on BES-II in the near future

will provide us more information about the QCD phase diagram.

The speed of sound, as one of fundamental properties of substance, can also convey QCD phase structure information. Lattice QCD, for instance, shows the local minimum value in c_s around the temperature $T_0 = 156.5 \pm 1.5$ MeV at vanishing baryon chemical potential [27, 28], which corresponds to a crossover transition between hadron gas and quark-gluon plasma (QGP). The numerical results from the effective models [29–31] suggest that the speed of sound is the global minimum at CEP, but it does not completely vanish in the mean field approximation. The speed of sound is one of the crucial physical quantities in hydrodynamics, which carries important information in describing the evolution of strongly interacting matter and final observables in heavy-ion collision experiments. The studies in [32–34] indicate that the speed of sound c_s as a function of charged particle multiplicity ($dN_{ch}/d\eta$) can be extracted from heavy-ion collision data. Recently, the authors [35] estimate the value of c_s as well as its logarithmic derivative with respect to the baryon number density, and try to build a connection with the cumulants of the baryon number distribution in matter created in heavy-ion collisions to aid in detecting the QCD CEP.

The first-order phase transition from the hadronic to quark matter at high baryon densities may also occur in the interior of massive neutron stars [36, 37]. Some recent studies have shown that quark-matter cores can appear in massive neutron stars [38–40]. Compared with the hadronic matter (HM), strange quark matter (SQM) is known to exhibit markedly different properties. For example, SQM at very high densities ($\rho_B \geq 40\rho_0$) is approximately scale invariant or conformal, whereas in HM the degree of freedom is smaller and the scale invariance

* liuhe@qut.edu.cn

† jumin@upc.edu.cn

‡ wuhaoyu@ysu.edu.cn

§ kyois@126.com

is also violated by the breaking of chiral symmetry. These qualitative differences between HM and SQM can be reflected in the speed of sound, where c_s takes the constant $c_s^2 = 1/3$ in the exactly conformal matter corresponding to SQM at high densities. However, c_s^2 in HM varies considerably: below saturation density, most hadronic models, such as chiral effective field theory, indicate $c_s^2 \ll 1/3$, while at higher densities the maximum of c_s^2 is predicted to be greater than 0.5 [41, 42]. Moreover, the behavior of c_s as a function of baryon number density influences the mass-radius relation, the tidal deformability and gravitational wave, and thus is helpful in understanding the equation of state (EOS) of neutron star matter and QCD phase structure. A recent research in Ref. [43] finds that the EOS with a pronounced peak in the speed of sound leaves a clear and unique signature in the main frequency of the postmerger gravitational wave (GW) spectrum, which can provide a sensitive probe of the hadron-quark phase transition in the dense core. On the other hand, the physical quantity that the polytropic index γ can also convey the qualitative differences between HM and SQM. The polytropic index has the value $\gamma = 1$ in conformal quark matter, while the hadronic models generically predict $\gamma = 2.5$ around the saturation density [44]. Some recent researches indicate the approximate rule that the polytropic index $\gamma < 1.75$ can be used as a good criterion for separating quark matter from hadronic matter in the massive neutron star core [38–40]. In Ref. [45], authors suggest that a more "conservative" criterion $\gamma \leq 1.6$ and $c_s^2 \leq 0.7$ can be used to determine the possible onset of the exotic matter (likely made of quark matter). Therefore, the polytropic index could convey information on the phase transition and provide a new probe to search the QCD CEP.

In the present study, we investigate the speed of sound and polytropic index of QCD matter in the full phase diagram based on a 3-flavor Polyakov-loop Nambu-Jona-Lasinio (pNJL) model. The definitions of the speed of sound and polytropic index require specifying which properties of the system are considered constant. In this work, we mainly calculate the speed of sound and polytropic index in the adiabatic and isothermal cases and analyze the changing behavior of these quantities around the chiral phase transition boundary and CEP. By constructing the hypothetical chemical freeze-out lines, we can find that both the speed of sound and polytropic index are close to zero near the CEP. The difference is that the speed of sound rapidly decreases near the CEP, followed by a small spinodal behavior, while the polytropic index exhibits a more pronounced dip structure as it approaches the CEP.

The thermodynamic potential density of the 3-flavor pNJL model at finite temperature T can be expressed

as [7, 11]

$$\begin{aligned} \Omega_{\text{pNJL}} = & \mathcal{U}(\Phi, \bar{\Phi}, T) - 2N_c \sum_{i=u,d,s} \int_0^\Lambda \frac{d^3p}{(2\pi)^3} E_i \\ & - 2T \sum_{i=u,d,s} \int \frac{d^3p}{(2\pi)^3} \{ \ln[1 + 3\Phi e^{-\beta(E_i - \mu_i)} \\ & + 3\bar{\Phi} e^{-2\beta(E_i - \mu_i)} + e^{-3\beta(E_i - \mu_i)}] \\ & + \ln[1 + 3\bar{\Phi} e^{-\beta(E_i + \mu_i)} \\ & + 3\Phi e^{-2\beta(E_i + \mu_i)} + e^{-3\beta(E_i + \mu_i)}] \} \\ & + G_S(\sigma_u^2 + \sigma_d^2 + \sigma_s^2) - 4K\sigma_u\sigma_d\sigma_s. \end{aligned} \quad (1)$$

In the above, the temperature-dependent effective potential $\mathcal{U}(\Phi, \bar{\Phi}, T)$ as a function of the Polyakov loop Φ and $\bar{\Phi}$ is expressed as [7]

$$\begin{aligned} \mathcal{U}(\Phi, \bar{\Phi}, T) = & -b \cdot T \{ 54e^{-a/T} \Phi \bar{\Phi} + \ln[1 - 6\Phi \bar{\Phi} \\ & - 3(\Phi \bar{\Phi})^2 + 4(\Phi^3 + \bar{\Phi}^3)] \}, \end{aligned} \quad (2)$$

with the parameters $a = 664$ MeV and $b = 0.03\Lambda^3$, which leads to simultaneous crossovers of chiral restoration and deconfinement around $T \approx 200$ MeV. In Eq.(1), the factor $2N_c$ with $N_c = 3$ represents the spin and color degeneracy, and $\beta = 1/T$. G_S is the strength of the scalar coupling, and the K term represents the six-point Kobayashi-Maskawa-t'Hooft (KMT) interaction which is required to break the axial $U(1)_A$ symmetry [46]. The energy E_i of quarks with flavor i is expressed as $E_i(p) = \sqrt{p^2 + M_i^2}$, where M_i represents the constituent quark mass. In the mean-field approximation (MFA), quarks can be taken as quasiparticles with constituent masses M_i , which is related to spontaneous chiral symmetry breaking. The constituent quark mass M_i is determined by the gap equation of

$$M_i = m_i - 2G_S\sigma_i + 2K\sigma_j\sigma_k, \quad (3)$$

where m_i is current quark mass, $\sigma_i = \langle \bar{q}_i q_i \rangle$ stands for quark condensate, and (i, j, k) is any permutation of (u, d, s) . In the present calculation, we adopt the values of parameters given in Ref. [47] as $m_u = m_d = 5.5$ MeV, $m_s = 135.7$ MeV, $G_S\Lambda^2 = 3.67$, $K\Lambda^5 = -9.29$, where $\Lambda = 631.4$ MeV is the cutoff value in the momentum integration.

In order to obtain the values of $\sigma_u, \sigma_d, \sigma_s, \Phi, \bar{\Phi}$ in pNJL model, the numerical calculation is based on the following equations

$$\frac{\partial \Omega_{\text{pNJL}}}{\partial \sigma_u} = \frac{\partial \Omega_{\text{pNJL}}}{\partial \sigma_d} = \frac{\partial \Omega_{\text{pNJL}}}{\partial \sigma_s} = \frac{\partial \Omega_{\text{pNJL}}}{\partial \Phi} = \frac{\partial \Omega_{\text{pNJL}}}{\partial \bar{\Phi}} = 0. \quad (4)$$

The pressure, number density, and entropy density can be derived using the thermodynamic relations in the grand canonical ensemble as

$$P = -\Omega_{\text{pNJL}}, \quad \rho_B = -\frac{\partial \Omega_{\text{pNJL}}}{\partial \mu_B}, \quad s = -\frac{\partial \Omega_{\text{pNJL}}}{\partial T}, \quad (5)$$

and energy density can be calculated as

$$\varepsilon = -P + Ts + \mu_B \rho_B. \quad (6)$$

The speed of sound is the velocity of a longitudinal compression wave propagating through the medium, which is a fundamental property of substance [35]. The general definition of speed of sound is $c_s^2 = \partial P / \partial \varepsilon$. It is worth noting that calculating the speed of sound requires specifying which thermodynamic variables are kept constant. For the QGP created in relativistic heavy-ion collisions, it evolves with constant entropy per baryon s/ρ_B , so that using the adiabatic speed of sound c_{s/ρ_B} is appropriate. Differently, the isothermal speed of sound c_T is widely used in neutron star matter. However, the study in Ref. [35] suggests that the cumulants of the baryon number distribution in heavy-ion collisions can be used to estimate the isothermal speed of sound squared and its logarithmic derivative with respect to the baryon number density. This result provides a new method for obtaining information about the QCD structure in heavy-ion collisions and neutron star studies. Using the Jacobian determinant method and thermodynamic relations, the c_{s/ρ_B}^2 and c_T^2 in terms of T and μ_B are respectively written as

$$c_{s/\rho_B}^2 = \frac{s\rho_B(\frac{\partial s}{\partial \mu_B})_T - s^2(\frac{\partial \rho_B}{\partial \mu_B})_T - \rho_B^2(\frac{\partial s}{\partial T})_{\mu_B} + \rho_B s(\frac{\partial \rho_B}{\partial T})_{\mu_B}}{(sT + \mu_B \rho_B)[(\frac{\partial s}{\partial \mu_B})_T(\frac{\partial \rho_B}{\partial T})_{\mu_B} - (\frac{\partial s}{\partial T})_{\mu_B}(\frac{\partial \rho_B}{\partial \mu_B})_T]}, \quad (7)$$

and

$$c_T^2 = \frac{\rho_B}{T(\frac{\partial s}{\partial \mu_B})_T + \mu_B(\frac{\partial \rho_B}{\partial \mu_B})_T}. \quad (8)$$

Meanwhile, the polytropic index is introduced in [38] $\gamma \equiv \partial \ln P / \partial \ln \varepsilon$ as a criterion for separating hadronic matter from quark matter (or the exotic matter) [38–40, 45, 48], which could convey information on the phase transition. For the adiabatic and isothermal processes, the polytropic index can be derived using the speed of sound formulas as

$$\gamma_{s/\rho_B} = \frac{\varepsilon}{P} c_{s/\rho_B}^2, \quad (9)$$

and

$$\gamma_T = \frac{\varepsilon}{P} c_T^2. \quad (10)$$

We first discuss the squared speed of sound in the $\mu_B - T$ plane based on the 3-flavor pNJL model. As shown in Fig. 1, we present the full contour map of the squared speed of sound c_T^2 (left panel) and c_{s/ρ_B}^2 (right panel). One can be seen that the values of both c_T^2 and c_{s/ρ_B}^2 in the chiral breaking region are mostly less than 0.1. After passing through the chiral phase transition boundary, both c_T^2 and c_{s/ρ_B}^2 rapidly increase with the restoration of chiral symmetry and gradually approach the value $c_s^2 = 1/3$ of conformal limit at the high temperature and baryon chemical potential. It is an expected

behavior since quark condensate rapidly approach vanish with chiral restoration, and thus the quark matter at high temperature and density from pNJL model can be viewed as non-interaction conformal matter. Different from quark matter, most hadronic models, e.g., an improved isospin- and momentum-dependent interaction (ImMDI) model, indicate that the nucleon interactions are proportional to the baryon density [49, 50], leading to a steady increase in the speed of sound until the speed of light limit at high baryon density. If the phase transition from hadronic matter to quark matter taken place, the value of speed of sound could have dramatic changes at a certain density. It is interesting that recent hybrid star research suggests that a sudden downward step change of the speed of sound occurs in the hadron-quark phase transition, and it is restored with the decrease of nucleon and lepton degrees of freedom in the high density quark phase [39, 40]. This dramatic change in the speed of sound may leave a clear and unique signature in the main frequency of the postmerger gravitational wave (GW) spectrum.

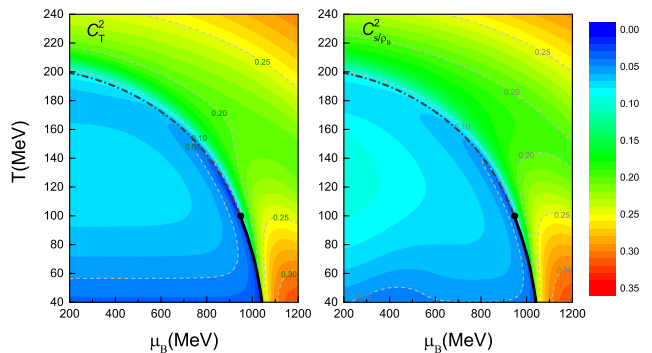


FIG. 1. (color online) the squared speed of sound c_T^2 (left) and c_{s/ρ_B}^2 (right) in the $\mu_B - T$ plane based on a 3-flavor pNJL model. The black dash-dotted and solid lines are respectively for the chiral crossover and first-order phase transition, the black dots connecting the chiral crossover and first-order phase transition represent the critical endpoints, and the gray dashed lines correspond to the contour of the squared speed of sound.

Another significant feature in Fig. 1 is that a dip structure in both c_T^2 and c_{s/ρ_B}^2 occurs at the low chemical potential side of the chiral phase transition. Especially around the first-order phase transition, the speed of sound rapidly decrease, and a global minimum value appears at the CEP. At low temperature and high chemical potential, there is a region where the values of c_T^2 and c_{s/ρ_B}^2 are relatively large, which is associated with the quarkyonic phase. This can be understood as a result of the fact that the chiral symmetry of light quarks is restored but the strange quark is still in chiral breaking. With the increase of chemical potential, the value of the speed of sound around the first-order phase transition of the strange quark decreases again, followed by another

increase in the speed of sound at the higher baryon chemical potential, and eventually approaching the conformal limit after the chiral restoration of strange quark.

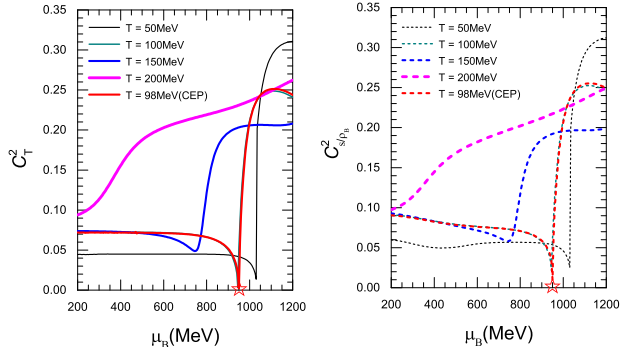


FIG. 2. (color online) the squared speed of sound c_T^2 (left) and c_{s/ρ_B}^2 (right) as functions of μ_B at $T = 50, 100, 150, 200$ MeV. The red stars mark the baryon chemical potential of the CEP.

To better characterize the variation of the speed of sound at the first-order phase transition, we plot in Fig. 2 the squared speed of sound c_T^2 and c_{s/ρ_B}^2 as functions of μ_B at a series of temperatures. We can see the very different behaviour of the speed of sound depending on whether a chiral phase transition occurs, and whether the chiral phase transition occurs through a smooth crossover or through a first-order phase transition. For the curve with $T = 200$ MeV above the chiral phase transition boundary, the speed of sound is monotonically increasing with the chemical potential. For the curve with $T = 150$ MeV, the speed of sound displays a spinodal behavior with a small dip around the smooth crossover. For the curve with $T < 100$ MeV, we can see a rapid dive and then a steep rise in c_T^2 and c_{s/ρ_B}^2 caused by the first-order phase transition. In particular, for the curve with $T = 98$ MeV, the points are shown as the red stars in Fig. 2 where the speed of sound in full phase diagram is global minimum and approaches to almost zero at the chemical potential $\mu_B = 950$ MeV. As can be seen in Fig. 1, the differences between c_T^2 and c_{s/ρ_B}^2 are mainly in the region of low temperatures and chemical potentials. Compared to c_T^2 , we can see in Fig. 2 a small decrease in c_{s/ρ_B}^2 at low chemical potentials. It is more worth pointing out that although the global minimum values of c_T^2 and c_{s/ρ_B}^2 occur at the CEP, neither of them are exactly zero, where the difference is that $c_{s/\rho_B}^2 = 0.01$ is slightly larger than $c_T^2 = 0.002$. The similar non-zero behavior of the adiabatic speed of sound at the CEP also exists in other modeling studies as result of the mean-field approximation [29–31].

Similarly, for the first time, we investigate the full contour map of the polytropic index γ_T and γ_{s/ρ_B} in the $\mu_B - T$ plane as shown in Fig. 3. It can be seen that the values of γ_T and γ_{s/ρ_B} are almost less than 1.5 in the

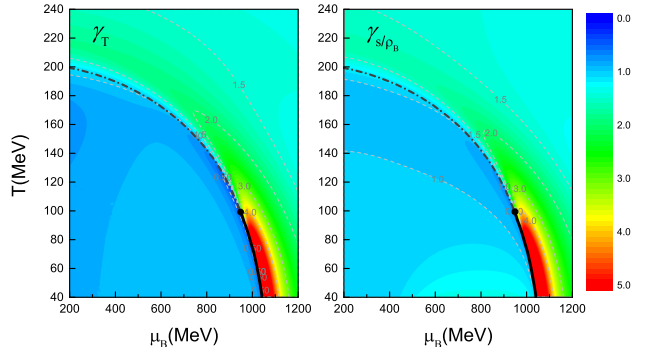


FIG. 3. (color online) The same as in Fig. 1, but for the polytropic index γ_T (left) and γ_{s/ρ_B} (right).

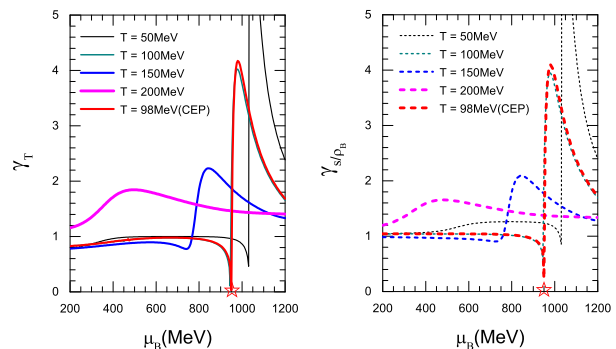


FIG. 4. (color online) The same as in Fig. 2, but for the polytropic index γ_T (left) and γ_{s/ρ_B} (right).

chiral breaking region, but increase rapidly to the maxima with chiral restoration and then decrease again to the value $\gamma = 1$ of conformal limit at high temperature and baryon chemical potential. The changing behaviors of the polytropic index γ_T and γ_{s/ρ_B} around the chiral phase transition boundary are illustrated in Fig. 4. For the curve with $T = 200$ MeV, different from the monotonic increase of the speed of sound with the chemical potential, both the two polytropic index increase to a maximum value and then gradually decrease to the conformal limit. Meanwhile, around the location of the chiral crossover and first-order phase transition, we can also find the nonmonotonic behaviour of the γ_T and γ_{s/ρ_B} with a dip and peak structure. This can be explained by formulas (9) and (10), where the polytropic index is equal to the squared speed of sound divided by the factor P/ε . The value of P/ε basically matches with that of the squared speed of sound for $\mu_B \ll \mu_{BC}$, where μ_{BC} is the baryon chemical potential of the chiral phase transition, and also goes close again at high baryon chemical potential, leading to that the polytropic index is close to 1. c_T^2 and P/ε isothermally measured in Ref. [51, 52] using the different models are consistent with our results. Except for these two regions, the squared speed of sound

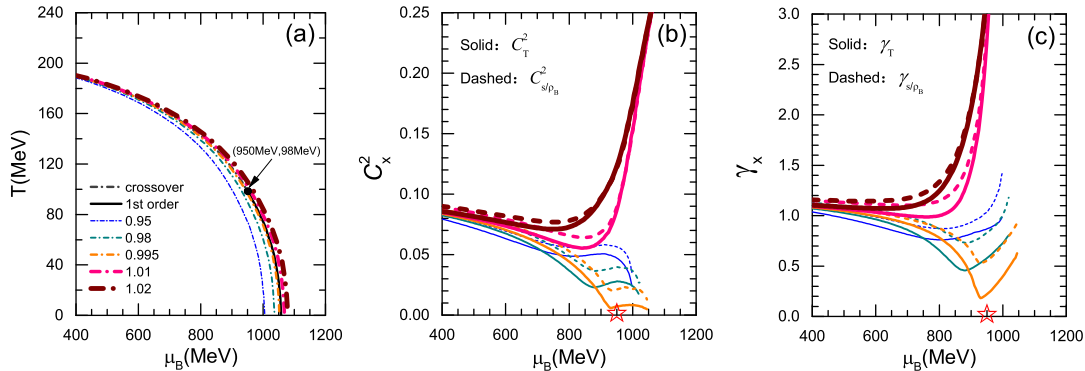


FIG. 5. (color online) The hypothetical chemical freeze-out lines (a) by rescaling μ_B of the chiral phase transition boundary with factors of 0.95, 0.98, 0.995, 1.01, and 1.02, as well as the squared speed of sound (b) and polytropic index (c) along the hypothetical chemical freeze-out lines. The black dash-dotted and solid lines in (a) are respectively for the crossover and first-order phase transition, but the solid and dashed lines in (b) and (c) represent the results of the speed of sound and polytropic index in adiabatic and isothermal cases, respectively. The black dot in (a) connecting the crossover and first-order phase transition represents the CEP, and the red stars in (b) and (c) mark the baryon chemical potential of the CEP.

(the derivative of P with respect to ε) does not match P/ε . Around the location of the chiral crossover, for instance, the local minima of these two quantities are not synchronized, making the minimum and maximum of the polytropic index appear at different chemical potentials. But for the first-order phase transition, the discontinuous changes in the quark condensate (chiral order parameter) are also reflected in the polytropic index, which rapidly increases from the minimum to the maximum at almost the same chemical potential. Similar to the speed of sound, the two types of polytropic index reach their minimum value at the CEP ($\mu_B = 950$ MeV, $T = 98$ MeV) but are not completely zero, where the value in adiabatic is greater than that in isothermal.

Some studies using the relativistic dissipative hydrodynamics show that the speed of sound as a function of charged particle multiplicity $\langle dN_{ch}/d\eta \rangle$ can be extracted from heavy-ion collision data [32–34]. The recent study in Ref. [35] also suggests that the net-baryon fluctuations in heavy-ion collisions can be used to estimate the isothermal speed of sound squared and its logarithmic derivative. In heavy-ion collision experiments, the net-baryon and net-charge fluctuations are measured at the chemical freeze-out. However, the location of the chemical freeze out cannot be well determined at RHIC-BES energies. There are several empirical criteria for the chemical freeze-out, such as fixed energy per particle at about 1 GeV, fixed total density of baryons and antibaryons, fixed entropy density over T^3 , as well as the percolation model and so on (see reference [53] and references therein). In order to compare qualitatively the speed of sound and polytropic index from the pNJL model with the (future) experimental results, we obtain the hypothetical chemical freeze-out lines by rescaling μ_B of the chiral phase transition boundary of light quarks with factors of 0.95, 0.98, 0.995, 1.01, and 1.02 corresponding

respectively to the color dash-dotted curves in Fig. 5 (a). The similar assumption of the chemical freeze-out lines was made in reference [13, 54]. We plot in Figs. 5 (b) and (c) the squared speed of sound and polytropic index along the hypothetical chemical freeze-out lines, where the solid and dashed lines represent the results in adiabatic and isothermal cases, respectively. For the hypothetical freeze-out lines over the chiral phase transition boundary, we can observe a rapid rise in the curves of both the squared speed of sound and polytropic index after a slight softening near the CEP. However, the speed of sound and the polytropic index along the hypothetical freeze-out lines below the chiral phase transition boundary vary considerably: the speed of sound rapidly decreases near the CEP, especially as c_T^2 approaches 0 along the curve with the factor of 0.995, followed by a small spinodal behavior and eventually continuing to decrease, while the polytropic index, especially γ_T , exhibits a more pronounced and nearly closed to zero dip structure as it approaches the CEP. Compared to the speed of sound, the polytropic index could provide a more sensitive probe of the QCD CEP in future experimental exploration.

In conclusion, we have investigated the speed of sound and polytropic index of QCD matter in the full phase diagram based on a 3-flavor Polyakov-looped Nambu-Jona-Lasinio (pNJL) model. In this work, we mainly calculate the speed of sound and polytropic index in the adiabatic and isothermal cases and analyze the changing behavior of these quantities near the CEP. As a result, we can find that a dip structure in both c_T^2 and c_{s/ρ_B}^2 occurs at the low chemical potential side of the chiral phase transition, and these two types of speed of sound have both reached their global minimum values at the CEP but are not completely zero, where the value in adiabatic is greater than that in isothermal. The polytropic index ex-

hibits similar behavior, but the difference is that it does not increase monotonically along any isothermal curve in the phase diagram. Especially around the location of the chiral crossover and first-order phase transition, we find the a dip and peak structure in the γ_T and γ_{s/ρ_B} . Along the hypothetical chemical freeze-out lines below the chiral phase transition boundary, the speed of sound rapidly decrease near the CEP, followed by a small spinodal behavior, while the polytropic index, especially γ_T , exhibits a more pronounced and nearly closed to zero dip structure as it approaches the CEP. Compared to the speed of sound, the polytropic index could provide a more sensitive probe of the QCD CEP in future experiment. However, the polytropic index at present is mainly applied to

the study of the massive neutron stars. The approximate rule that $\gamma < 1.75$ [38] or $\gamma \leq 1.6$ and $c_s^2 \leq 0.7$ [45] can be used as a good criterion for separating quark matter from hadronic matter in the massive neutron star core. Further, it is worth looking forward to some observations related to the polytropic index being found and applied to the search for critical endpoint in heavy-ion collisions and the study of gravitational wave.

This work is supported by the National Natural Science Foundation of China under Grants No. 12205158, No. 11975132, and No. 12305148, as well as the Shandong Provincial Natural Science Foundation, China Grants No. ZR2021QA037, No. ZR2022JQ04, No. ZR2019YQ01, and No. ZR2021MA037.

-
- [1] Y. Aoki, G. Endrődi, Z. Fodor, S.D. Katz, and K.K. Szabó, *Nature (London)* **443** (2006) 675.
- [2] S. Gupta, X.F. Luo, B. Mohanty, H.G. Ritter, and N. Xu, *Science* **332** (2011) 1525.
- [3] S. Borsányi, Z. Fodor, C. Hoelbling, S.D. Katz, S. Krieg, and K.K. Szabó, *Phys. Lett. B* **730** (2014) 99.
- [4] T.M. Schwarz, S.P. Klevansky, and G. Papp, *Phys. Rev. C* **60** (1999) 055205.
- [5] P. Zhuang, M. Huang, and Z. Yang, *Phys. Rev. C* **62** (2000) 054901.
- [6] W.J. Fu, Z. Zhang, and Y.X. Liu, *Phys. Rev. D* **77** (2008) 014006.
- [7] K. Fukushima, *Phys. Rev. D* **77** (2008) 114028; K. Fukushima, *Phys. Rev. D* **78** (2008) 039902 (E).
- [8] S.X. Qin, L. Chang, H. Chen, Y.X. Liu, and C.D. Roberts, *Phys. Rev. Lett.* **106** (2011) 172301.
- [9] B. J. Schaefer and M. Wagner, *Phys. Rev. D* **85** (2012) 034027.
- [10] J.W. Chen, J. Deng, H. Kohyama, and L. Labun, *Phys. Rev. D* **93** (2016) 034037.
- [11] H. Liu, J. Xu, L.W. Chen, K.J. Sun, *Phys. Rev. D* **94** (2016) 065032.
- [12] W.J. Fu, J.M. Pawłowski, and F. Rennecke, *Phys. Rev. D* **101** (2020) 054032.
- [13] H. Liu, J. Xu, *Universe* **7** (2021) 6.
- [14] M. M. Aggarwal, et al., (STAR Collaboration), *Phys. Rev. Lett.* **105** (2010) 022302.
- [15] L. Adamczyk, et al., (STAR Collaboration), *Phys. Rev. Lett.* **112** (2014) 032302.
- [16] J. Adam, et al., (STAR Collaboration), *Phys. Rev. Lett.* **126** (2021) 092301.
- [17] M. Abdallah, et al., (STAR Collaboration), *Phys. Rev. C* **104** (2021) 024902.
- [18] L. Adamczyk, et al., (STAR Collaboration), *Phys. Rev. C* **92** (2015) 014904.
- [19] J. Adam, et al., (STAR Collaboration), *Phys. Rev. C* **103** (2021) 034908.
- [20] L. Adamczyk, et al., (STAR Collaboration), *Phys. Rev. Lett.* **112** (2014) 162301.
- [21] L. Adamczyk, et al., (STAR Collaboration), *Phys. Rev. Lett.* **120** (2018) 062301.
- [22] M.I. Abdulhamid, et al., (STAR Collaboration), *Phys. Lett. B* **845** (2023) 138165.
- [23] M.I. Abdulhamid, et al., (STAR Collaboration), *Phys. Rev. Lett.* **130** (2023) 202301.
- [24] K.J. Sun, L.W. Chen, C.M. Ko, J. Pu, and Z. Xu, *Phys. Lett. B* **781** (2018) 499.
- [25] K.J. Sun, C.M. Ko, F. Li, J. Xu, and L.W. Chen, *Eur. Phys. J. A* **57** (2021) 313.
- [26] K.J. Sun, F. Li, and C.M. Ko, *Phys. Lett. B* **816** (2021) 136258.
- [27] A. Bazavov et al. (HotQCD Collaboration), *Phys. Lett. B* **795** (2019) 15.
- [28] S. Borsanyi, Z. Fodor, J. N. Guenther, et al., *Phys. Rev. Lett.* **125** (2020) 052001.
- [29] M. Motta, R. Stiele, W. M. Alberico, and A. Beraudo, *Eur. Phys. J. C* **80** (2020) 770.
- [30] W.B. He, G.Y. Shao, X.Y. Gao, X.R. Yang, and C.L. Xie, *Phys. Rev. D* **105** (2022) 094024.
- [31] W.B. He, G.Y. Shao, and C.L. Xie, *Phys. Rev. C* **107** (2023) 014903.
- [32] H.C. Song, S.A. Bass, U. Heinz, T. Hirano, and C. Shen, *Phys. Rev. Lett.* **106** (2011) 192301.
- [33] H.C. Song, S.A. Bass, and U. Heinz, *Phys. Rev. C* **83** (2011) 024912.
- [34] P. Deb, G.P. Kadam, and H. Mishra, *Phys. Rev. D* **94** (2016) 094002.
- [35] A. Sorensen, D. Oliinychenko, V. Koch, and L. McLerran, *Phys. Rev. Lett.* **127** (2021) 042303.
- [36] N. K. Glendenning, *Phys. Rep.* **342** (2001) 393.
- [37] F. Weber, *Prog. Part. Nucl. Phys.* **54** (2005) 193.
- [38] E. Annala, T. Gorda, A. Kurkela, J. Nättilä, and A. Vuorinen, *Nat. Phys* **16** (2020) 907.
- [39] H. Liu, X.M. Zhang, and P.C. Chu, *Phys. Rev. D* **107** (2023) 094032.
- [40] H. Liu, Y.H. Yang, Y. Han, and P.C. Chu, *Phys. Rev. D* **108** (2023) 034004.
- [41] S. Gandolfi, A.Y. Illarionov, K.E. Schmidt, F. Pederiva, and S. Fantoni, *Phys. Rev. C* **79** (2009) 054005.
- [42] I. Tews, T. Krüger, K. Hebeler, and A. Schwenk, *Phys. Rev. Lett.* **110** (2013) 032504.
- [43] Y.J. Huang, L. Baiotti, T. Kojo, K. Takami, H. Sotani, H. Togashi, T. Hatsuda, S. Nagataki, and Y.Z. Fan, *Phys. Rev. Lett.* **129** (2022) 181101.
- [44] A. Kurkela, P. Romatschke, and A. Vuorinen, *Phys. Rev. D* **81** (2010) 105021.
- [45] M.Z. Han, Y.J. Huang, S.P. Tang, and Y.Z. Fan, *Sci. Bull.* **68** (2023) 913.

- [46] G. t'Hooft, Phys. Rev. D **14** (1976) 3432; G. t'Hooft, Phys. Rev. D **18** (1978) 2199 (E).
- [47] T. Hatsuda and T. Kunihiro, Phys. Rep. **247** (1994) 221.
- [48] T. Malik and C. Providência, Phys. Rev. D **106** (2022) 063024.
- [49] J. Xu, L.W. Chen, and B.A. Li, Phys. Rev. C **91** (2015) 014611.
- [50] J. Xu, A. Carbone, Z. Zhang, and C.M. Ko, Phys. Rev. C **100** (2019) 024618.
- [51] A.A. Khan, et al., Phys. Rev. D **64** (2001) 074510.
- [52] S.K. Ghosh and T.K. Mukherjee, Phys. Rev. D **73** (2006) 114007.
- [53] J. Cleymans, H. Oeschler, K. Redlich, S. Wheaton, Phys. Rev. C **73** (2006) 034905.
- [54] J.W. Chen, J. Deng, H. Kohyama, L. Labun, Phys. Rev. D **95** (2017) 014038.